Rai, A.C., Lin, C.-H., and Chen, Q. 2015. "Numerical modeling of particle generation from ozone reactions with human-worn clothing in indoor environments," *Atmospheric Environment*, 102, 145-155.

Numerical modeling of particle generation from ozone reactions with human-worn clothing in indoor environments

Aakash C. Rai[1], Chao-Hsin Lin[2], & Qingyan Chen[3,1*]

[1]School of Mechanical Engineering, Purdue University, West Lafayette, IN 47907, USA
[2]Environmental Control Systems, Boeing Commercial Airplanes, Everett, WA 98203, USA
[3]School of Environmental Science and Engineering, Tianjin University, Tianjin 300072, China

[*]Tel. (765)496-7562, Fax (765)494-0539, Email: yanchen@purdue.edu

Abstract

Ozone-terpene reactions are important sources of indoor ultrafine particles (UFPs), a potential health hazard for human beings. Humans themselves act as possible sites for ozone-initiated particle generation through reactions with squalene (a terpene) that is present in their skin, hair, and clothing. This investigation developed a numerical model to probe particle generation from ozone reactions with clothing worn by humans. The model was based on particle generation measured in an environmental chamber as well as physical formulations of particle nucleation, condensational growth, and deposition. In five out of the six test cases, the model was able to predict particle size distributions reasonably well. The failure in the remaining case demonstrated the fundamental limitations of nucleation models. The model that was developed was used to predict particle generation under various building and airliner cabin conditions. These predictions indicate that ozone reactions with human-worn clothing could be an important source of UFPs in densely occupied classrooms and airliner cabins. Those reactions could account for about 40% of the total UFPs measured on a Boeing 737-700 flight. The model predictions at this stage are indicative and should be improved further.

Keywords: Ozone, Skin-oils, Particles, Nucleation, Condensation, Indoor environment

1. Introduction

Particulate air pollution is a matter of serious health concern for humans. Several studies have associated exposure to outdoor particles with increased morbidity and mortality risks (Dominici et al., 2006; Pope and Dockery, 2006). However, outdoor exposure to particles is usually less significant than indoor exposure because people spend the majority of their time indoors. Therefore, it is presumable that many of the adverse health effects that are apparently due to outdoor particles are actually caused by exposure indoors (Jones, 1999). Hence, it is imperative to characterize people's exposure to particles in indoor environments.

Several investigations have identified ozone reactions with terpene-containing consumer products as an important source of indoor particles (Sarwar and Corsi, 2007; Weschler and Shields, 1999). For example, Long et al. (2000) found that ozone/terpene reactions drastically increased (with a peak increase of 7–100 times) the particle number concentrations in Boston-area homes. They also found that more than 50% of those particles (by volume) were ultrafine in nature. Such ultrafine particles (UFPs) can deposit deep into the lungs and presumably are responsible for many of the adverse health effects associated with particles (Donaldson et al.,

1998; Sioutas et al., 2005). Hence, several researchers focused on measuring UFP generations from ozone/terpene reactions (Coleman et al., 2008; Destaillats et al., 2006). They found that such reactions were indeed a major source of indoor UFPs. A recent investigation has identified ozone reactions with squalene (a triterpene) present in human skin-oils as another potential source of indoor UFPs (Wang and Waring, 2014).

In addition to experimental investigations, some researchers have developed models for predicting particle generation from ozone/terpene reactions on the basis of detailed chemical mechanisms (Leungsakul et al., 2005; Sarwar et al., 2003). These models can provide reasonable predictions of particle mass generation. However, they cannot compute particle number concentrations and size distributions, which are essential indices for characterizing exposure to UFPs (Donaldson et al., 1998; Peters et al., 1997). A recent study by Ito and Harashima (2011) developed a sectional model for simulating particle generation from ozone reactions with d-limonene (a terpene) together with particle size distributions. However, their model did not include condensational growth, which is the predominant mechanism for increase in particle size in such reactions.

Therefore, to better understand ozone-initiated particle generation and human exposure to the particles, this investigation developed a numerical model for computing size-resolved particle concentrations based on physical formulations of particle dynamics. We used the model to analyze particle generation from ozone reactions with human-worn clothing, which were recently identified as a potential source of indoor UFPs (Rai et al., 2013). The model was then used to compute concentrations of such ozone-initiated particles in various indoor environments such as buildings and airliner cabins.

2. Method

This investigation simulated the generation of ozone-initiated particles from reactions with human-worn clothing as measured in an environmental chamber. The details of the chamber experiments were provided in Rai et al. (2013) and are briefly summarized here. Figure 1 shows the schematic of the chamber and the anticipated particle-generation mechanism. Experiments were conducted in a medium-scale environmental chamber (dimensions: 1.8 m × 1.7 m × 1.7 m) containing a steel box (dimensions: 0.2 m × 0.4 m × 1.2 m.) at its center. The box was used as a human simulator, with its temperature maintained at 31±1 °C and a cotton T-shirt stretched over it. The T-shirt was soiled with skin-oils by a human subject's sleeping in it and was the primary site for ozone reactions. The chamber was ventilated with outdoor air enriched with ozone, which reacted with the T-shirt to generate particles. The experiments measured the time-varying concentrations of ozone and particles at the chamber inlet and exhaust. The measurements therefore presented a well-controlled and challenging case study for developing models to study ozone-initiated particle generation from the reaction of ozone with clothing.

To model particle generation, this investigation assumed that ozone reacted with skin-oils on the T-shirt to produce a hypothetical semi-volatile organic compound (SVOC) in the vapor phase, as shown in Figure 1. Our assumption was based on the fact that skin-oil constituents such as squalene react with ozone and produce SVOCs (Fadeyi et al., 2013). The concentration of the SVOC vapor then increased in the chamber because its production rate from ozone/skin-oil reactions was higher than its removal rate by ventilation and deposition. The SVOC vapor

concentration subsequently crossed its nucleation threshold, and new particles (liquid droplets of SVOC) were generated. Note that if ventilation and deposition rates were sufficiently high, particle generation would not take place because the SVOC vapor concentration would never cross its nucleation threshold.

These freshly nucleated particles then served as condensation sites for the SVOC vapor and subsequently reduced its concentration below the nucleation threshold, preventing further nucleation. From this time onward, condensation was predominant, which led to growth in particle size and consumption of the SVOC vapor. Furthermore, the number of particles in the chamber was also decreasing because nucleation had stopped and particles were continuously removed by ventilation and deposition, as illustrated in Figure 1. This in turn reduced the number of available condensation sites for the SVOC vapor, and its concentration started to increase again, producing another nucleation burst of particles. This cycle of particle generation, growth, and removal continued until the ozone/skin-oil reactions could not generate sufficient SVOC vapor in the chamber. Note that coagulation of particles was ignored in the above description because the particle concentrations in most cases were too low for coagulation to have a significant influence (Hussein et al., 2009).

2.1 Model formulation

As described above, the SVOC vapor was the primary driver of the particle generation cycle. The SVOC concentration in the chamber was assumed to be under well-mixed conditions. The mass conservation equation for the SVOC is as follows:

$$\frac{dC_{SVOC}}{dt} = S_{gen} - \lambda_v C_{SVOC} - \lambda_{d,SVOC} C_{SVOC} - CS \cdot C_{SVOC} - \rho \frac{\pi}{6} Dp_{nuc}^3 J_{nuc} \quad (1)$$

where C_{SVOC} is the concentration of SVOC vapor [kg m^{-3}], t the time [s], S_{gen} the SVOC production rate [kg m^{-3} s^{-1}], λ_v the air change rate [s^{-1}], $\lambda_{d,SVOC}$ the SVOC deposition rate coefficient on the chamber walls [s^{-1}], CS the condensational sink of SVOC vapor on the existing particles [s^{-1}] (see Section 2.1.3 for details), ρ the particle density [kg m^{-3}], Dp_{nuc} the diameter of nucleating particles [m], and J_{nuc} the particle nucleation rate [# m^{-3} s^{-1}].

The first term in the above equation is the rate of change of SVOC concentration in the chamber. The second term describes the production of SVOC from ozone/skin-oil reactions. The third and fourth terms describe SVOC removal by ventilation and deposition, respectively. The fifth and sixth terms are the SVOC conversion rates of particles from vapor to liquid droplets as a result of condensation and nucleation, respectively. Clearly, the above equation can be used to determine the time-varying SVOC vapor concentration in the chamber if the various terms on the right-hand side are computed. However, the equation is intrinsically coupled with the particle concentrations through the condensation and nucleation sink terms.

Therefore, it is necessary to introduce governing equations for particles. Just as the mass balance equation was used for the SVOC vapor, this investigation used the number balance equation to compute the particle number concentrations in the chamber. The particles were first classified into different groups on the basis of diameter, and their number concentrations were computed by the following equations:

$$\frac{dN(Dp_i,t)}{dt} = -\lambda_v N(Dp_i,t) - \lambda_{d,p}(Dp_i)N(Dp_i,t) + J_{nuc} \quad (\text{for } i = 1)$$
$$\frac{dN(Dp_i,t)}{dt} = -\lambda_v N(Dp_i,t) - \lambda_{d,p}(Dp_i)N(Dp_i,t) \qquad (\text{for } i = 2, 3, ...) \tag{2}$$

where i is the group number, N the number concentration of particles [# m^{-3}] with diameters Dp_i [m] at time t, $\lambda_{d,p}$ their deposition rate coefficient [s^{-1}], and Dp_{nuc} the diameter of nucleating particles [m]. The first term in each of the above equations is the rate of change of particle number concentration with diameter Dp_i. The second and third terms describe the removal of particles by ventilation and deposition, respectively. The fourth term expresses particle generation by nucleation of SVOC vapor, which is a source of nucleating particles (i = 1 and Dp_1 = Dp_{nuc}) only. Note that the above equations do not include the incoming particles from ventilation and that we chose those experimental cases for which the inlet air contained negligible particles for comparison with the numerical results. Although inlet particles do not pose any theoretical problems and can be easily incorporated into Eq. (2), they increase computational costs drastically by increasing the number of groups in the model, and therefore they were not considered. We also did not account for coagulation in Eq. (2) because it was usually insignificant as a result of low particle concentrations.

To solve Eq. (2) for computing size-resolved particle concentrations, it is also necessary to account for particle size growth as described by Kumar and Ramkrishna (1997). The growth of particle diameters was governed by the condensation of SVOC vapor, which was computed by the following expression (Kulmala, 1988):

$$\frac{dDp_i}{dt} = \frac{4\beta \cdot D \cdot C_{SVOC}}{\rho Dp_i} \tag{3}$$

where D is the diffusion coefficient of SVOC in air [m^2 s^{-1}] and β the transition correction factor (Fuchs and Sutugin, 1971).

Overall, Eqs. (1), (2), and (3) can be used for computing the time-dependent SVOC vapor concentration, particle number concentrations, and particle diameters, respectively. However, the various terms on the right-hand side of these equations needed to be determined, as described in the following subsections.

2.1.1 Modeling the SVOC generation (S_{gen})

The ozone-initiated SVOC generation (S_{gen} in Eq. (1)) was estimated by assuming a heterogeneous second-order reaction between ozone and skin-oils on the T-shirt as follows:

$$\text{Ozone} + \text{Skin-oils} \xrightarrow{k_{ozone}} SVOC_{vapor}$$

Thus, the generation rate of SVOC was expressed as:

$$S_{gen} = \frac{k_{ozone} A_{T-shirt} C_{skin-oils} C_{ozone}}{V} \tag{4}$$

where k_{ozone} is the ozone/skin-oils reaction rate constant [s^{-1} ppb^{-1}]; $A_{T\text{-}shirt}$ the area of the T-shirt [m^2]; V the chamber volume [m^3]; and C_{ozone} and $C_{skin\text{-}oils}$ the concentrations of ozone in the air [ppb] and skin-oils on the T-shirt [kg m^{-2}], respectively. The determination of ozone/skin-oils-reaction-generated SVOC was based on the assumption that the T-shirt was soiled with skin-oils because it was worn by a human subject. We calculated the time-varying concentration of skin-oils by solving the following equation:

$$\frac{dC_{skin-oils}}{dt} = -k_{ozone} C_{skin-oils} C_{ozone} \quad (5)$$

Clearly, the above equation can be easily solved if the initial concentration of skin-oils on the T-shirt ($C_{0,skin\text{-}oils}$), C_{ozone}, and k_{ozone} are known. C_{ozone} was measured during the experiments; however, $C_{0,skin\text{-}oils}$ and k_{ozone} were not known beforehand. Therefore, this investigation fitted those two constants by comparing the model predictions for ozone-initiated particles with their corresponding measurements, as described in the Supplementary Information (SI). Finally, Eqs. (4) and (5) can be solved for computing S_{gen}.

The above calculation method for S_{gen} can be simplified if it is assumed that the T-shirt contained a large reservoir of skin-oils and that the reactions were controlled only by the ozone concentration in the chamber. Then the expression for S_{gen} becomes:

$$S_{gen} = \frac{k_{ozone-ex} A_{T-shirt} C_{ozone}}{V} \quad (6)$$

where $k_{ozone\text{-}ex}$ is the ozone/skin-oils reaction rate constant with the assumption of excess skin-oils [kg m^{-2} s^{-1} ppb^{-1}]. Again, $k_{ozone\text{-}ex}$ can be estimated by comparing the model predictions with measurements as described in the SI.

This study used both of the methods described above for computing S_{gen} and also compared their performance in simulating ozone-initiated particles, as analyzed in the results section. The calculation of S_{gen} from Eqs. (4) and (5) was termed the "skin-oils depletion" model, and the calculation of S_{gen} from Eq. (6) was termed the "excess skin-oils" model.

2.1.2. Modeling the nucleation rate (J_{nuc})

Nucleation governs the generation rate of new particles from ozone/skin-oil reactions. Hence, the aim of any nucleation model is to predict the generation rate of new particles given the physical properties of the nucleating species (SVOC vapor in this study), its super-saturation, and other environmental conditions. Various nucleation theories are described in detail in many texts (Seinfeld and Pandis, 2006), so our discussion here will be brief.

The nucleation rate can be determined experimentally if the generation of freshly nucleated particles is measured. However, such particles have extremely small sizes (on the order of a few nanometers) and usually cannot be detected by conventional measurement instruments such as a scanning mobility particle sizer (SMPS). Therefore, particles are measured only when they grow beyond the detection size limit, which is usually about ten nanometers. For example, the detection range for the SMPS used in our ozone/T-shirt experiments was between

9.65–421.7 nm, which means that the true nucleation rate was unknown. Nevertheless, these SMPS measurements can be used to compute the generation rate of the smallest detectable particles, also called the apparent nucleation rate (Kerminen and Kulmala, 2002).

To calculate the apparent nucleation rate, we summed Eq. (2) over all particle sizes and performed some algebraic manipulations given in the SI, which led to the following expression:

$$J_{nuc,app} \approx \frac{dN_{total,SMPS}(t)}{dt} + \lambda_v . N_{total,SMPS}(t) + \sum_{Dp_i = Dp_{SMPS}}^{\infty} \lambda_{d,p}(Dp_i).N(Dp_i, t) \quad (7)$$

where $J_{nuc,app}$ is the apparent nucleation rate, $N_{total,SMPS}$ the total particle number concentration measured by SMPS [# m^{-3}], and Dp_{SMPS} the smallest particle diameter detected by the SMPS (9.65 nm).

Finally, to compute $J_{nuc,app}$, Eq. (7) can be solved jointly with Eqs. (1) to (3) by using $N_{total,SMPS}$ from the measured data. However, we first need to replace Dp_{nuc} with Dp_{SMPS} and J_{nuc} with $J_{nuc,app}$ in Eqs. (1) and (2) because those particles with diameters below Dp_{SMPS} were eliminated from the model formulation and were accounted for indirectly through the $J_{nuc,app}$ term in Eq. (7). Such an approach was extremely useful for studying the evolution of particle sizes after they were detected by the SMPS. It was also useful to compare the model results with measurements of particle size distributions for validating Eqs. (1) to (3).

The primary limitation of the above approach was that $J_{nuc,app}$ need to be computed at every time-step from the measured $N_{total,SMPS}$ in an environmental chamber in which ozone/T-shirt reactions were the only particle source. A similar technique would not be possible in real indoor settings because the measured $N_{total,SMPS}$ would also contain contributions from other particle-generating sources. Therefore, it was necessary to explore a number of theoretical models for nucleation that did not require $N_{total,SMPS}(t)$ as an input. However, the nucleation precursors and mechanism of particle generation from ozone/clothing reactions is itself unknown. Therefore, we chose several popular nucleation models from the literature and compared their performance in order to identify the most suitable model. The models studied were the thermodynamic, kinetic, and activation nucleation models.

The thermodynamic model is based on the classical homogenous nucleation theory, which is derived from the thermodynamic theory of fluctuations. A widely used expression for nucleation rate is the following, which is based on work by Volmer and Weber (1926), Farkas (1927), Becker and Döring (1935), Zeldovich (1942), and Frenkel (1955):

$$J_{nuc} = \left(\frac{2\sigma}{\pi m^5}\right)^{1/2} \frac{v C_{SVOC}^2}{S} \exp\left(\frac{-16\pi}{3k^3} \frac{v^2\sigma^3}{T^3(\ln S)^2}\right) \quad (8)$$

where σ is the surface tension of the SVOC [kg s^{-2}], m the molecular mass of SVOC [kg], v (v = m/ρ) the molecular volume of particles [m^3], S the super-saturation ratio, k the Boltzmann constant [1.38×10^{-23} m^2 kg s^{-2} K^{-1}], and T the air temperature [K]. The super-saturation ratio of the SVOC is defined as $S=C_{SVOC}/C_{SVOC,sat}$, where $C_{SVOC,sat}$ is the SVOC concentration in a saturated vapor at equilibrium [kg m^{-3}].

Another popular theory of nucleation is the kinetic theory, which assumes that nucleation is determined by the collision rate of molecules rather than by the thermodynamic criterion (Lushnikov, 2010). The nucleation rate is given by:

$$J_{nuc} = k_{kin} C_{SVOC}^2 \quad (9)$$

where k_{kin} is the kinetic nucleation constant [m^3 kg^{-2} s^{-1}].

Recently, the activation nucleation theory was proposed by Kulmala et al. (2006) for explaining atmospheric nucleation events. It was also used by Vartiainen et al. (2006) to compute nucleation of particles from ozone/d-limonene reactions in an indoor environment. Therefore, it was chosen as another possible candidate for computing nucleation. This theory assumes that nucleation occurs through the activation of existing thermodynamically stable clusters by SVOCs, and the nucleation rate is given by:

$$J_{nuc} = k_{act} C_{SVOC} \quad (10)$$

where k_{act} is the activation nucleation constant [kg^{-1} s^{-1}].

2.1.3. Modeling the condensational sink (CS) and deposition rate coefficients ($\lambda_{d,SVOC}$ and $\lambda_{d,p}$).

The condensational sink (CS) determines the rate of SVOC condensation on existing particles. For the condensational growth governed by Eq. (3), CS is given by the following expression (Kulmala et al., 2001):

$$CS = 2\pi D \sum_i \beta . Dp_i . N(Dp_i) \quad (11)$$

The SVOC deposition coefficient ($\lambda_{d,SVOC}$) on the chamber walls was computed from Lai and Nazaroff's (2000) deposition model, as suggested by Weschler and Nazaroff (2008). The particle deposition coefficient ($\lambda_{d,p}$) on the chamber walls was assumed to be constant (0.25 h^{-1}) for all diameters since a more sophisticated deposition modeling was not possible due to the lack of data for size-resolved deposition velocities at the chamber walls.

2.2 Estimating physical and modeling constants

The solutions of the model equations (Eqs. (1) – (11)) require appropriate values for the physical properties of the hypothetical SVOC and particles as well as the various modeling constants. However, those physical properties and modeling constants could only be estimated because the particle generation mechanism from ozone/skin-oils reactions is not well studied and the SVOCs responsible for particle generation are themselves unknown. Table 1 shows the values used in this investigation and our estimation methodology is given in the SI.

3. Results and discussions

This section first reports the simulation results for ozone-initiated particle generations from reactions with soiled clothing obtained by using the apparent nucleation formulation (Eq.

(7)) and their comparison with chamber measurements conducted by Rai et al. (2013). These comparisons were useful for evaluating the performance of the various model formulations used in this investigation, except for the nucleation model, because Eq. (7) computed the nucleation from the measurements themselves (i.e., the measurements of $N_{total,SMPS}$). However, as discussed previously, it is not practical to use such an approach for computing ozone/clothing-generated particles under realistic indoor conditions, since their individual contributions to particles cannot be isolated from other particle sources. Therefore, we subsequently replaced the apparent nucleation model with different theoretical nucleation models that can compute ozone-initiated particles without the measurement of $N_{total,SMPS}$. We then evaluated the performance of the thermodynamic, kinetic, and activation nucleation models by comparing their predictions with the corresponding measurements. Finally, we used the thermodynamic model to estimate the ozone-initiated particle generation from human clothing under typical building and airliner cabin conditions, because performance of this model was found to be superior to that of the other two models.

3.1. Apparent nucleation rate formulation

Because nucleation modeling was the most difficult aspect of this research, we computed the apparent nucleation rates from Eq. (7). To reduce computational expenses, our model assumed that the inlet air contained a negligible number of particles. Therefore, to test the model formulations, we chose those cases from the measurements of Rai et al. (2013) which had low inlet particle concentrations. The experimental conditions for these cases are summarized in Table 2. The cases systematically analyzed the impact of various factors on ozone-initiated particle generation, such as ozone concentration, soiling degree of the T-shirt, and air change rate. They were designed by keeping Case 2 as the reference case and typically varying one condition at a time.

Among these cases, we studied Cases 1-4 with the apparent nucleation formulation. We could not study Cases 5 and 6 with this approach because particle generation was not detected in these cases, which meant that Eq. (7) could not be used for computing the nucleation rate ($J_{nuc,app}$). These two cases were used for studying the performance of the various nucleation models, which is discussed in the next subsection.

Figure 2 compares the computed and measured ozone-initiated particle number concentrations for Cases 1, 3, and 4. The measurements showed that the ozone-initiated particle numbers were negligible from t = 0 to t = 2.5 h because the ozone concentration was very low (~5 ppb). Particle generation was measured about one hour after ozone injection through a burst of nucleation, and the total number concentrations reached a maximum. The particle numbers then started to decay because of the lack of nucleation and because of particle removal by ventilation and deposition. A secondary burst of nucleation was clearly observed in cases with high ozone concentrations, and the particle numbers showed secondary maxima. The secondary burst was not detected under low ozone conditions, mainly because of the large measurement uncertainties. Finally, the particle numbers decayed further, and the experiments were terminated at t = 12.5 h.

As shown in Figure 2 for the “excess skin-oils” model, the computed particle number concentrations were in excellent agreement with the measurements at different ozone levels,

primarily because the apparent nucleation rate was estimated from the measurements themselves. Note that in the case of 148 ppb ozone, the model over-predicted the number concentrations by about 10–15% from t = 5.2 h to t = 8.5 h. This case had particle concentrations in excess of 10,000 #/cm^3, meaning that coagulation could be responsible for a reduction in particle number (Hussein et al., 2009). The fact that coagulation was not included in our model probably led to slight over-prediction. We also obtained excellent agreement in the 40 ppb ozone case (results not shown). The results with the "skin-oils depletion" model were almost identical to the "excess skin-oils" model and therefore are not shown here.

Figure 3(a) shows the particle mass concentrations obtained by the two SVOC generation models for the 40 ppb and 148 ppb ozone cases (Cases 2 and 4) and their comparisons with measurements. In both cases, the measured mass concentrations first increased as a result of particle generation after ozone injection, and then decayed toward the end. In the case of 40 ppb ozone, both models predicted the particle mass concentrations reasonably well when compared with the measurements, but the "excess skin-oils" model seemed to provide slightly better predictions than the "skin-oils depletion" model. However, with 148 ppb ozone, the "excess skin-oils" model hugely over-predicted the particle masses, while the "skin-oils depletion" model performed much better, although it still over-predicted the mass concentration by about 30%. Thus, it seems that the soiled T-shirt contained a limited quantity of skin-oils available for ozone reactions. These were consumed faster at the higher ozone concentration, and the T-shirt was significantly depleted of skin-oils, especially at later times.

In the case of 57 ppb ozone (Case 3), the trends of the results for particle mass concentrations from both models were similar to those in the previous cases, as shown in Figure 3(b). In this case, the T-shirt was soiled for 12 hours, as compared with 6 hours in the previous cases, which means that the quantity of skin-oils in the T-shirt was probably higher. Thus, the performance of the "excess skin-oils model" was somewhat better than that of the skin-oils depletion model, although it still slightly over-predicted the mass concentrations towards the end. We did not make comparisons for mass concentrations in the 22 ppb ozone (Case 1) because there were large uncertainties in the measurements of particle masses at this low ozone level (Rai et al., 2013).

Overall, the "skin-oils depletion" model seemed more suitable for simulating ozone-initiated particle generations from the soiled T-shirt over the human simulator because (1) its predictions of particle mass concentration agreed reasonably well with the measurements for all three cases analyzed, and (2) it correctly captured the decreasing trend of particle masses towards the end of the experiments, particularly in the case of 148 ppb ozone. However, it seems that the "excess skin-oils" model would be more appropriate for simulating particle generation with clothing worn by human beings, because the skin-oils would be replenished by human activities. The various discrepancies between the computed and measured values of mass concentration arose because (1) the T-shirt most likely did not contain the same amount of skin-oils in all cases, while the "skin-oils depletion" model assumed otherwise; and (2) the model assumed a second-order reaction between ozone and skin-oils, whereas the actual reaction is very complex.

Figure 4 compares the particle size distributions computed by the "skin-oils depletion" model with the corresponding measurements at an ozone concentration of 40 ppb (Case 2). The details of the particle generation, growth, and removal phenomena were provided in our previous

paper (Rai et al., 2013), and we briefly describe those results here for the purpose of comparison with model predictions.

As shown in Figure 4(a), ozone-initiated particles were generated in the ultrafine region with a mode diameter of approximately 40 nm at t = 4.2 h, and this was predicted reasonably well by the model. At t = 6.2 h, the particle mode diameter shifted to 90 nm as a result of condensational growth, and the number of particles was also depleted by ventilation and deposition losses; these phenomena were also well captured by the model. At t = 8.5 h, the particle size distribution was predominantly bimodal, with modes at 40 nm and 136 nm as shown in Figure 4(b). The former mode (40 nm) resulted from a secondary nucleation burst, and the latter (136 nm) was due to condensational growth of the original mode. The model predictions also showed two dominant modes and an overall good match with the measurements. From t = 8.5 h to 12.5 h, the particle concentrations decayed because of ventilation and deposition, and there were no obvious modes in the size distribution at t = 12.5 h. The model prediction also showed decay in particle concentrations, and the overall size distribution was again predicted reasonably well.

Evidently, the model captured the overall trend of particle generation, growth, and removal with good accuracy for the 40 ppb ozone case described above. The model performed slightly worse for the other cases (Cases 1, 3, and 4), but those predictions still compared well with their corresponding measurements. It should be emphasized that the model contained physical formulations for SVOC generation, condensation, and SVOC and particle deposition with few fitting constants. Hence, these model formulations seemed reasonable, given the good agreement between model predictions and experimental measurements. However, the apparent nucleation rate was computed from the experimental data itself (i.e, the measured $N_{total,SMPS}$), which was a big drawback in applying the model under new indoor conditions. Moreover, even if the $N_{total,SMPS}$ were obtained through measurement, there would be no way to separate the contributions of particles generated from ozone/clothing reactions from those from other indoor sources. Therefore, it was desirable to incorporate a suitable nucleation model for simulating ozone-initiated particles without aid from experimental measurements, as discussed in the next subsection.

3.2. Nucleation models

This section discusses the results obtained by using the different theoretical nucleation models described in Section 2.1.2: the activation, kinetic, and thermodynamic nucleation models. We again used the "skin-oils depletion" model to compute the results for this section because its performance was found to be superior to that of the "excess skin-oils" model.

As illustrated in the SI, the modeling constants in the various nucleation models were chosen such that the peak of the particle number concentration (at t = 4.2 h) in the reference case (40 ppb ozone) was captured reasonably well. Thus, all the nucleation models provided a good prediction of the maximum particle concentration in the case of 40 ppb ozone, as shown in Figure 5(a). However, none of the nucleation models could effectively capture the steep decline in particle number from t = 4.2 h to t = 7.0 h and the subsequent secondary nucleation burst. In the case of 148 ppb ozone, the thermodynamic model over-predicted the peak particle concentration by about 30%, whereas the kinetic and activation models under-predicted it by

about 10% and 40%, respectively, as shown Figure 5(b). Subsequently, all the models over-predicted the number concentrations, but the overall trend was better captured by the thermodynamic model than by the other two models.

Figure 6 compares the particle number concentrations obtained by different nucleation models with their corresponding measurements for Cases 5 and 6 conducted at high air change rates with different ozone concentrations. In both cases, particle generation was not measured. However, the different nucleation models generally predicted particle generation, as shown in Figures 6(a) and (b). In the case of 51 ppb ozone, the predictions of the thermodynamic model were the best, and those of the activation model were the worst. However, the opposite was true in the case of 133 ppb ozone. All the nucleation models failed overall in these cases, especially at the higher ozone concentration.

For Cases 1 and 3, all the nucleation models generally over-predicted the particle number concentrations. For example, the activation, kinetic, and thermodynamic models over-predicted the peak particle concentrations by about 400%, 260%, and 60%, respectively, in Case 1; and by about 10%, 30%, and 40% in Case 3. By and large, the thermodynamic model performed the best, and the activation model performed the worst in these cases.

In contrast to the significantly different predictions obtained for number concentrations by the various nucleation models, the predicted mass concentrations were similar among the three models, as shown in Figure 7 for the 40 ppb and 148 ppb ozone cases. In all the other cases that were analyzed, the particle mass concentrations generally were not very sensitive to the choice of nucleation model. This result was reasonable because mass transfer from vapor to liquid particles is determined primarily by condensation, and nucleation plays a secondary role. The reasons for the discrepancies between the model predictions and measurements (as seen in Figure 7) were discussed previously and can be attributed to the assumptions used in the "excess skin-oils" model.

Figure 8 compares the particle size distributions calculated by the different nucleation models with their corresponding measurements at several instants of time in the case of 40 ppb ozone. At $t = 4.2$ h, all the models predicted the particle size distributions reasonably well, as shown in Figure 8(a). At $t = 6.2$ h, the predictions by the thermodynamic and kinetic model seem reasonable, but those by the activation model are quite poor when compared with the measurements. The model predictions become much worse at $t = 8.5$ h and 12.5 h, as shown in Figures 8(c) and (d), respectively, and none of the models could reasonably capture the secondary nucleation burst.

It was also illustrative to compare Figures 4 and 8 for identifying the differences between the results obtained from the apparent nucleation formulation and the various theoretical nucleation models. After the theoretical nucleation models were introduced in place of the apparent nucleation approach, the computed results showed significant deterioration when compared to the measurements. Therefore, an accurate nucleation model is vital for correctly computing the size-resolved particle concentrations generated from ozone reactions with human-worn clothing.

In Cases 1, 3, and 4, the comparisons between particle size distributions predicted by the different nucleation models and their corresponding measurements were similar to the comparisons obtained in Case 2 (40 ppb ozone). In Cases 5 and 6, all the models predicted particle generation, but no generation was observed in the experiments. Hence, all the nucleation models failed in these two cases. The discrepancies can be attributed primarily to the unknown nucleation precursors and mechanism as well as the limitations of the different nucleation theories (Anisimov, 2003; Seinfeld and Pandis, 2006).

We also conducted a sensitivity analysis to identify the impact of physical and modeling constants on the results predicted by using the thermodynamic nucleation model since this model had the best performance. The results of our sensitivity analysis are given in the SI. Our analysis revealed that the model predictions for particle numbers were extremely sensitive to the values of σ, m, and ρ, whereas the particle masses were less sensitive to changes in physical and modeling constants. Overall, it was found that the developed model should be used cautiously and the results should be treated as indicative only, especially when computing particle number concentrations.

3.3 Ozone-initiated particles under different indoor environments

In spite of the disagreement between the model predictions and measurements, it was seen that the thermodynamic nucleation model worked reasonably well in five out of six cases. Hence, we used this model to simulate particle generation from ozone reactions with occupant's clothing in the following indoor settings: a classroom, office, and home as building environments, and Boeing 737-700 and Boeing 777 airliner cabins as airplane environments.

The detailed results for the building environments can be found in SI, and we briefly summarize them here. We first studied a typical classroom (with 25 pupils and one teacher) described in Fischer et al. (2013) at various air change rates (from 0.1–10.0 ACH) under two different outdoor ozone levels (50 ppb and 100 ppb) with and without background particles. The maximum ozone-initiated UFP concentration was 6000 #/cm^3, obtained at 2.0 ACH under 100 ppb outdoor ozone levels in the absence of background particles. In addition to classroom conditions, we also studied particle generation for typical office and home environments. These cases assumed the same conditions as in the classroom, except that there were four occupants in the office and two in the home. UFP generation in the office and home was much lower because the reduced occupancy resulted in lower ozone reactions. Even under conditions that were favorable for new particle generation, the maximum UFP concentration was only 400 #/cm^3 for the office and 40 #/cm^3 for the home, obtained at 1 ACH under 100 ppb outdoor ozone levels in the absence of background particles. Hence, it seems ozone/clothing generated UFPs would be significant only under high occupancy conditions such as classrooms.

Since the ozone/clothing generated UFPs were found to be maximum under high ozone and occupancy conditions without background particles, we also studied those particle generations in airliner cabins that usually have such conditions. This investigation simulated UFP generation from ozone/clothing reactions in a fully occupied Boeing-777 flight for a duration of 10 hours without background particle at 50 ppb cabin ozone concentration. The flight is typically trans-continental. It was predicted that the flight would have significant UFP generation, and the time-averaged particle concentration was computed as 6800 #/cm^3.

Next, we conducted a case study for a typical domestic flight of 1.5 hours. The flight was made by a partially occupied B737-700 airliner for which ozone-initiated UFP generation was recently measured by Spengler et al. (2012). The measured ozone and particle concentrations very quite low initially, as shown in Figure 9. After 15 minutes, the ozone concentration started to increase, and after another five minutes the particle concentrations also rose steeply. The particle concentration then remained steady throughout the cruising portion of the flight. Finally, the ozone and particles decayed sharply during the descent. Figure 9 also shows the contributions of UFPs generated from ozone reactions with the passengers' clothing as computed by our model. These reactions can account for about 40% of the total UFPs measured. Obviously, other ozone-initiated mechanisms of particle generation must have prevailed, such as the reaction of ozone with various terpene-containing consumer products, but taking these reactions into account was beyond the scope of this investigation. Nevertheless, the model results indicate that ozone reaction with passengers' clothing could be a significant contributor of UFPs under typical airliner cabin conditions.

4. Conclusions

This investigation developed numerical models to study particle generation from the reaction of ozone with human-worn clothing. The models were developed with the use of: (1) experimental measurements of particle generation in an environmental chamber; (2) two new approaches developed for modeling the SVOC generation from ozone/clothing reactions; and (3) physical formulations for particle nucleation, growth, and removal mechanisms taken from literature. The models can predict size-resolved particle number concentrations, and they have provided insights into the overall particle-generation mechanism.

The UFP predictions with the apparent nucleation formulation were in good agreement with the experimental data, in which the "nucleation rate" was directly estimated from the measured particle concentrations. However, the numerical models in combination with different theoretical nucleation models displayed significant discrepancies in predicting the UFP size distributions because of some fundamental limitations of the nucleation models. Overall, the thermodynamic model based on the classical homogeneous nucleation theory provided the most reasonable predictions for five out of the six experimental cases.

Finally, the thermodynamic model was used to compute particle generation from ozone reactions with human-worn clothing in different building and airplane environments. The results show that ozone reactions could significantly contribute to UFP generation in high-occupancy spaces such as classrooms and airliner cabins. Ozone/clothing reactions may have accounted for about 40% of the UFPs measured in a Boeing 737-700 flight. However, their contributions to UFPs in office and home environments did not seem to be important because of the low occupant density.

Acknowledgements

This study was partially supported by the National Basic Research Program of China (The 973 Program) through Grant No. 2012CB720100 and the Center for Cabin Air Reformative Environment (CARE) at Tianjin University, China. The investigation was also partially funded by the U.S. Federal Aviation Administration (FAA) Office of Aerospace Medicine through the

National Air Transportation Center of Excellence for Research in the Intermodal Transport Environment at Purdue University under Cooperative Agreement 10-C-RITE-PU. Although the FAA sponsored this project, it neither endorses nor rejects the findings of the research. This information is presented in the interest of invoking comments from the technical community about the results and conclusions of the research.

References

Anisimov, M.P., 2003. Nucleation: theory and experiment. Russ. Chem. Rev. 72, 591–628.

Becker, R., Döring, W., 1935. Kinetische behandlung der keimbildung in übersättigten dampfen, Ann. Phys. (Leipzig) 24, 719-752.

Coleman, B.K., Lunden, M.M., Destaillats, H., Nazaroff, W.W., 2008. Secondary organic aerosol from ozone-initiated reactions with terpene-rich household products. Atmos. Environ. 42, 8234–8245.

Destaillats, H., Lunden, M.M., Singer, B.C., Coleman, B.K., Hodgson, A.T., Weschler, C.J., Nazaroff, W.W., 2006. Indoor secondary pollutants from household product emissions in the presence of ozone: a bench-scale chamber study. Environ. Sci. Technol. 40, 4421–4428.

Dominici, F., Peng, R.D., Bell, M.L., Pham, L., McDermott, A., Zeger, S.L., Samet, J.M., 2006. Fine particulate air pollution and hospital admission for cardiovascular and respiratory diseases. JAMA, J. Am. Med. Assoc. 295, 1127–1134.

Donaldson, K., Li, X.Y., MacNee, W., 1998. Ultrafine (nanometre) particle mediated lung injury. J. Aerosol Sc. 29, 553–560.

Fadeyi, M.O., Weschler, C.J., Tham, K.W., Wu, W.Y., Sultan, Z.M., 2013. Impact of human presence on secondary organic aerosols derived from ozone-initiated chemistry in a simulated office Environment. Environ. Sci. Technol. 47, 3933–3941.

Farkas, L., 1927 Keimbildungsgeschwindigkeit in übersättigen dämpfen, Z Phys. Chem. 125, 236–242.

Fischer, A., Ljungström, E., Langer, S., 2013. Ozone removal by occupants in a classroom. Atmos. Environ. 81, 11–17.

Frenkel, J., 1955. Kinetic theory of liquids. Dover, New York.

Fuchs, N.A., Sutugin, A.G., 1971. Topics in current aerosol research. Pergamon, New York.

Hussein, T., Hruška, A., Dohányosová, P., Džumbová, L., Hemerka, J., Kulmala, M., Smolík, J., 2009. Deposition rates on smooth surfaces and coagulation of aerosol particles inside a test chamber. Atmos. Environ. 43, 905–914.

Ito, K., Harashima, H., 2011. Coupled CFD analysis of size distributions on indoor secondary organic aerosol derived from ozone/limonene reactions. Build. Environ. 46, 711–718.

Jones, A.P., 1999. Indoor air quality and health. Atmos. Environ. 33, 4535–4564.

Kerminen, V.-M., Kulmala, M., 2002. Analytical formulae connecting the “real” and the “apparent” nucleation rate and the nuclei number concentration for atmospheric nucleation events. J. Aerosol Sc. 33, 609–622.

Kulmala, M., 1988. Nucleation as an aerosol physical problem (Ph.D. thesis). University of Helsinki, Helsinki, Finland.

Kulmala, M., Lehtinen, K.E.J., Laaksonen, A., 2006. Cluster activation theory as an explanation of the linear dependence between formation rate of 3nm particles and sulphuric acid concentration. Atmos. Chem. Phys. 6, 787–793.

Kulmala, M., Maso, M.D., Mäkelä, J.M., Pirjola, L., Väkevä, M., Aalto, P., Miikkulainen, P., Hämeri, K., O'dowd, C.D., 2001. On the formation, growth and composition of nucleation mode particles. Tellus B 53, 479–490.

Kumar, S., Ramkrishna, D., 1997. On the solution of population balance equations by discretization—III. Nucleation, growth and aggregation of particles. Chem. Eng. Sci. 52, 4659–4679.

Lai, A.C.K., Nazaroff, W.W., 2000. Modeling indoor particle deposition from turbulent flow onto smooth surfaces. J. Aerosol Sc. 31, 463–476.

Leungsakul, S., Jaoui, M., Kamens, R.M., 2005. Kinetic mechanism for predicting secondary organic aerosol formation from the reaction of d-limonene with ozone. Environ. Sci. Technol. 39, 9583–9594.

Long, C.M., Suh, H.H., Koutrakis, P., 2000. Characterization of indoor particle sources using continuous mass and size monitors. J. Air Waste Manage. Assoc. 50, 1236–1250.

Lushnikov, A.A., 2010. Condensation, evaporation, nucleation, in: Agranovski, I. (Ed.), Aerosols - Science and Technology. Wiley-VCH Verlag GmbH & Co. KGaA, 91–126.

Peters, A., Wichmann, H.E., Tuch, T., Heinrich, J., Heyder, J., 1997. Respiratory effects are associated with the number of ultrafine particles. Am. J. Respir. Crit. Care Med. 155, 1376–1383.

Pope, C.A., Dockery, D.W., 2006. Health effects of fine particulate air pollution: lines that connect. J. Air Waste Manage. Assoc. 56, 709–742.

Rai, A.C., Guo, B., Lin, C.-H., Zhang, J., Pei, J., Chen, Q., 2013. Ozone reaction with clothing and its initiated particle generation in an environmental chamber. Atmos. Environ. 77, 885–892.

Sarwar, G., Corsi, R., 2007. The effects of ozone/limonene reactions on indoor secondary organic aerosols. Atmos. Environ. 41, 959–973.

Sarwar, G., Corsi, R., Allen, D., Weschler, C., 2003. The significance of secondary organic aerosol formation and growth in buildings: experimental and computational evidence. Atmos. Environ. 37, 1365–1381.

Seinfeld, J.H., Pandis, S.N., 2006. Atmospheric chemistry and physics: from air pollution to climate change. John Wiley & Sons.

Sioutas, C., Delfino, R.J., Singh, M., 2005. Exposure assessment for atmospheric Ultrafine Particles (UFPs) and implications in epidemiologic research. Environ. Health Perspect. 113, 947–955.

Spengler, J.D., Vallarino, J., McNeely, E., Estephan, H., 2012. In-flight/onboard monitoring: ACER's component for ASHRAE 1262, Part 2 (No. RITE - ACER - CoE - 2012 - 6). Harvard School of Public Health, Boston, MA.

Vartiainen, E., Kulmala, M., Ruuskanen, T.M., Taipale, R., Rinne, J., Vehkamäki, H., 2006. Formation and growth of indoor air aerosol particles as a result of d-limonene oxidation. Atmos. Environ. 40, 7882–7892.

Volmer, M., Weber, A., 1926. Keimbildung in übersättigten gebilden, Z. Phys. Chem. 119, 277–301.

Wang, C., Waring, M.S., 2014. Secondary organic aerosol formation initiated from reactions between ozone and surface-sorbed squalene. Atmos. Environ. 84, 222–229.

Weschler, C.J., Nazaroff, W.W., 2008. Semivolatile organic compounds in indoor environments. Atmos. Environ. 42, 9018–9040.

584 Weschler, C.J., Shields, H.C., 1999. Indoor ozone/terpene reactions as a source of indoor
585 particles. Atmos. Environ. 33, 2301–2312.
586 Zeldovich, Y. B., 1942. Theory of new-phase formation: cavitation. J. Exp. Theor. Phys. (USSR)
587 12, 525–538.

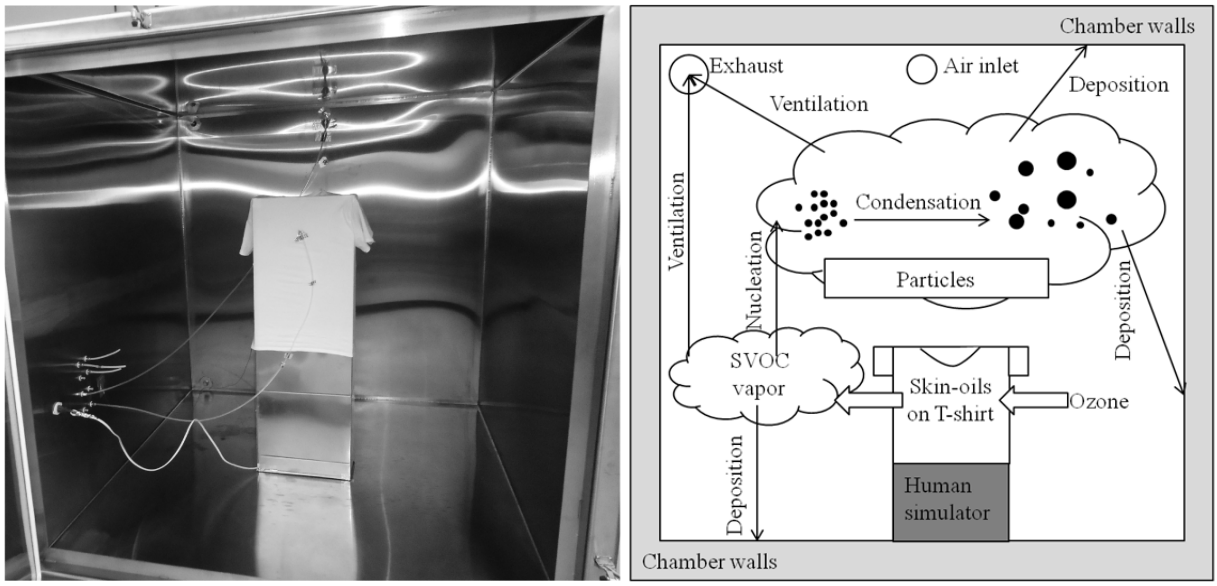

Fig. 1. Schematic of the environmental chamber used to study ozone reactions with a T-shirt on a human simulator and an illustration of the particle-generation mechanism.

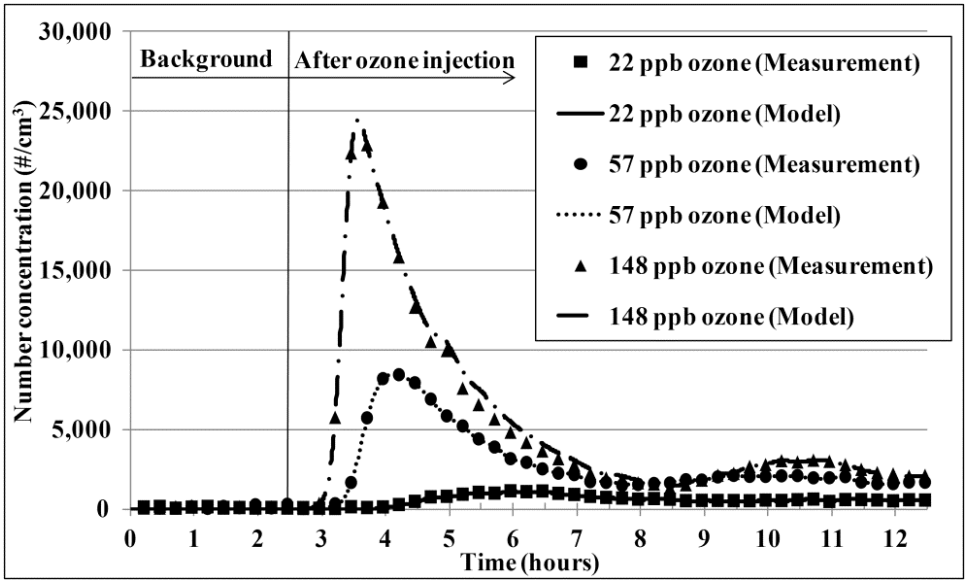

Fig. 2. Comparison of particle number concentrations computed by the "excess skin-oils" model with the corresponding measurements at different ozone concentrations.

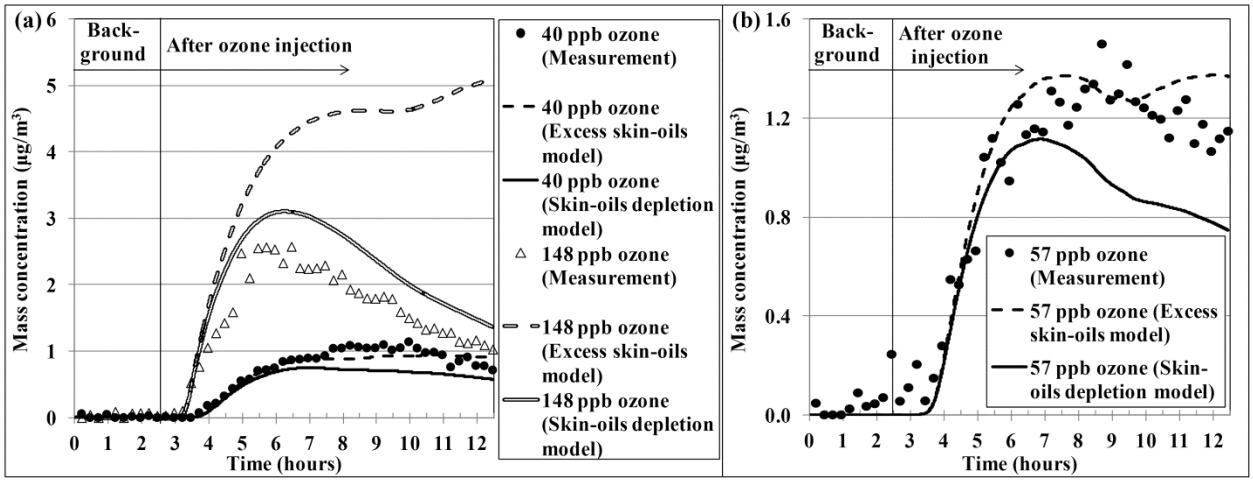

Fig. 3. Comparisons of particle mass concentrations computed by the "excess skin-oils" and "skin-oils depletion" models with the corresponding measurements at (a) 40 ppb and 148 ppb ozone with 6 hours of T-shirt soiling, and (b) 57 ppb ozone with 12 hours of T-shirt soiling.

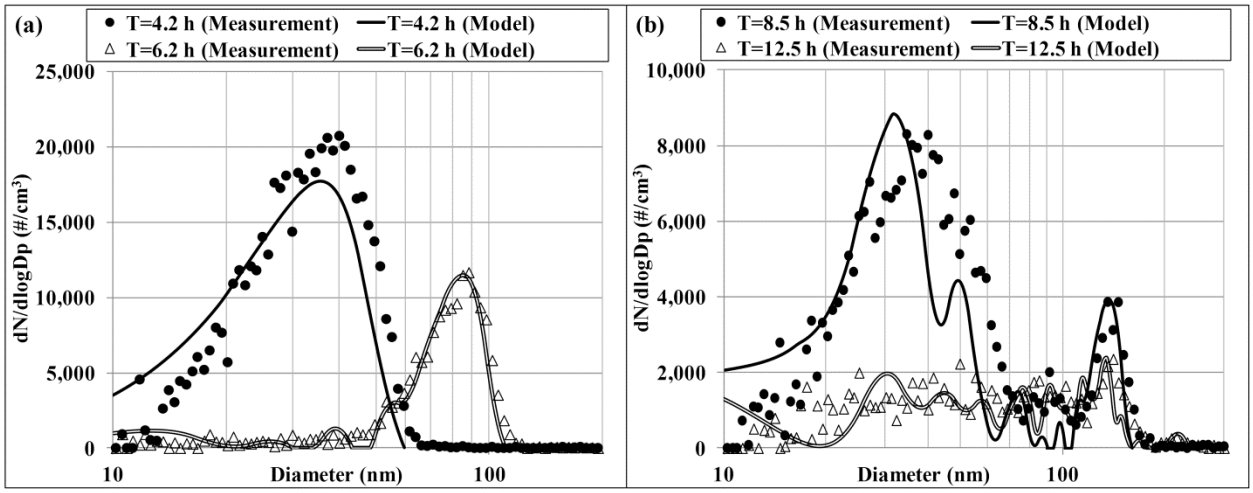

Fig. 4. Comparisons of particle size distributions computed by the "skin-oils depletion" model with the corresponding measurements at an ozone concentration of 40 ppb for (a) t = 4.2 h and 6.2 h, and (b) t = 8.5 h and 12.5 h.

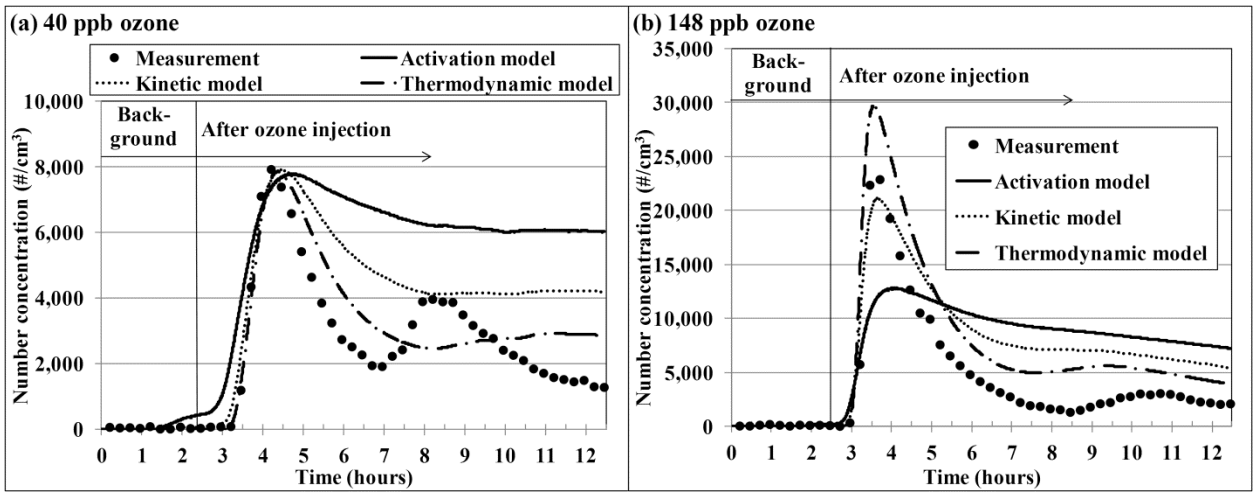

Fig. 5. Comparisons of particle number concentrations computed by the different nucleation models with the corresponding measurements at 0.5 ACH with (a) 40 ppb ozone and (b) 148 ppb ozone.

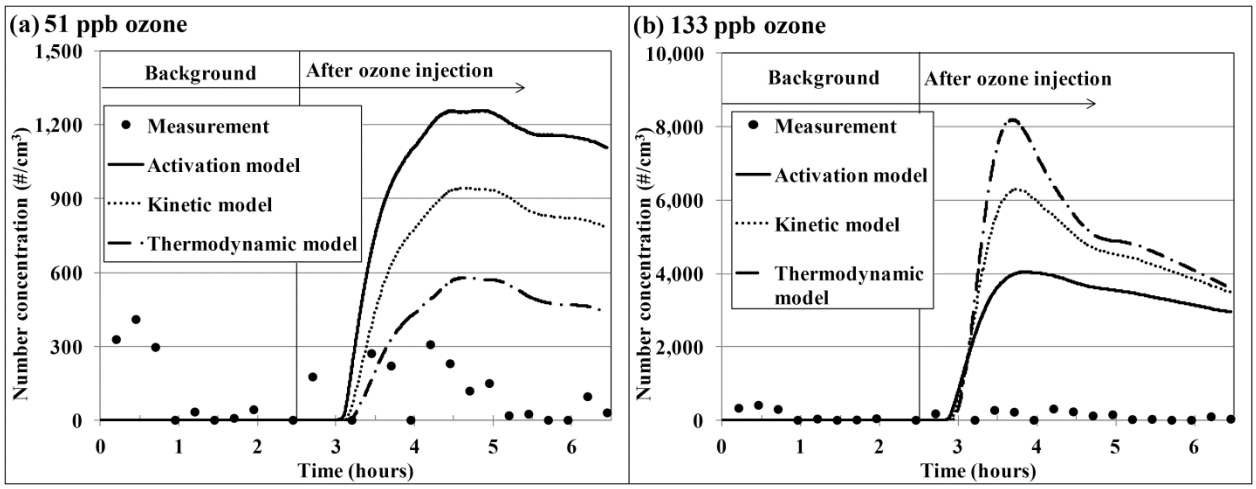

Fig. 6. Comparisons of particle number concentrations computed by the different nucleation models with the corresponding measurements at 2.7 ACH with (a) 51 ppb ozone and (b) 133 ppb ozone.

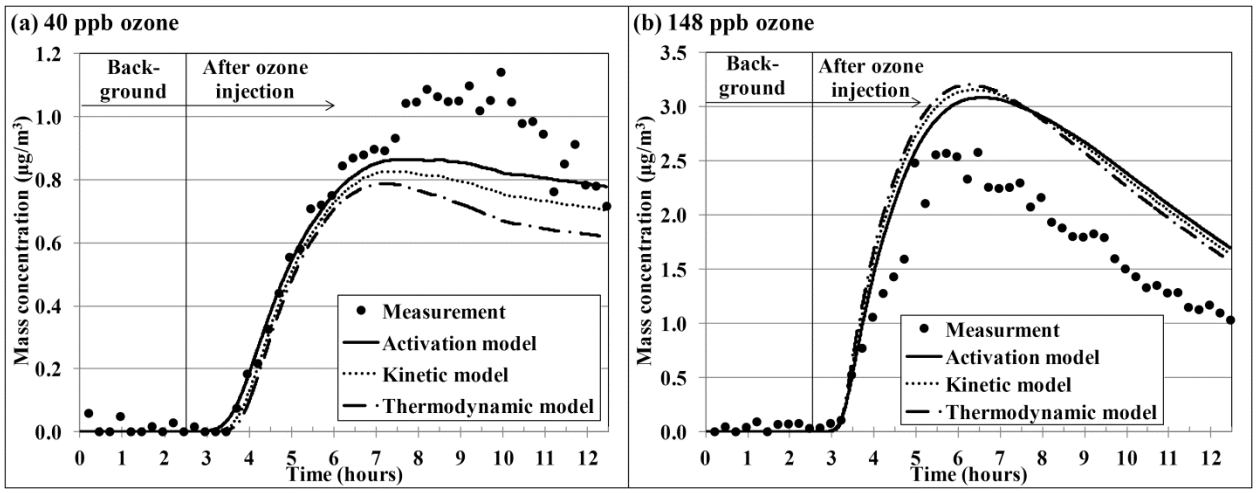

610
611 **Fig. 7.** Comparisons of particle mass concentrations computed by the different nucleation models
612 with the corresponding measurements at (a) 40 ppb ozone and (b) 148 ppb ozone.

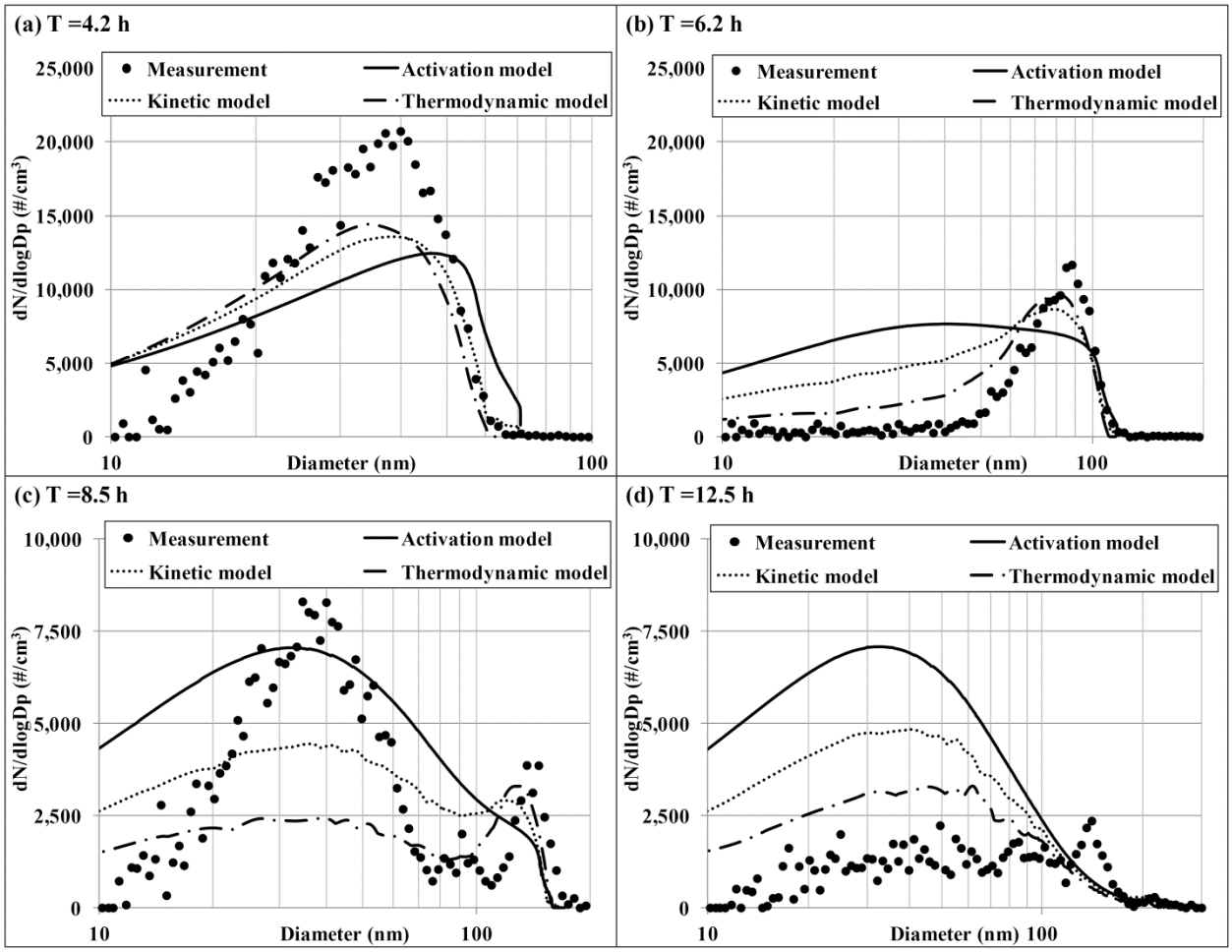

613
614 **Fig. 8.** Comparisons of particle size distributions computed by the different nucleation models
615 with the corresponding measurements at 40 ppb concentration for (a) t = 4.2 h, (b) t = 6.2 h, (c) t
616 = 8.5 h, and (d) t = 12.5 h.

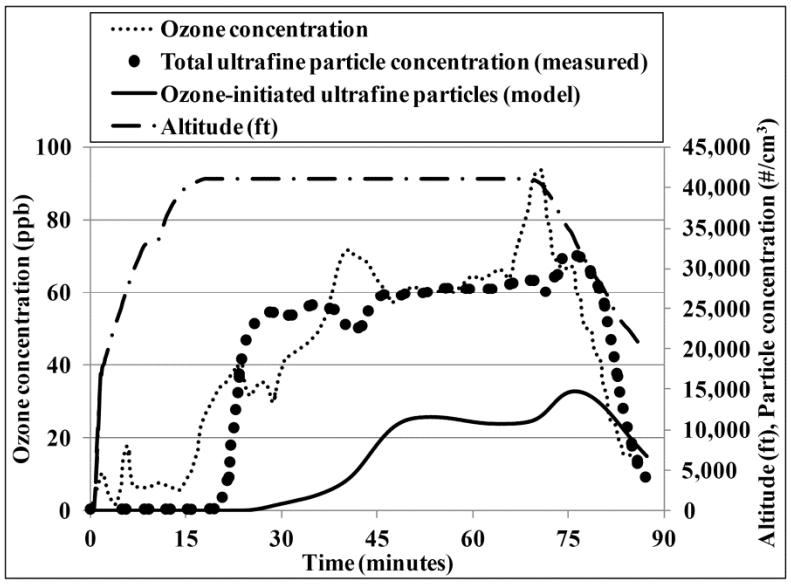

Fig. 9. Measurements of the ozone-initiated UFPs in a Boeing 737-700 flight and the corresponding contributions by ozone reactions with passengers' clothing as computed by the model.

621 **Table1.** Various physical and modeling constants used in this investigation

Variable	Estimated value	Variable	Estimated value
ρ	1.2 g cm^{-3}	D	5×10^{-6} m^2 s^{-1}
$k_{ozone\text{-}ex}$	2×10^{-10} kg m^{-2} h^{-1} ppb^{-1}	$C_{SVOC,sat}$	1×10^{-13} kg m^{-3}
k_{ozone}	1×10^{-3} h^{-1} ppb^{-1}	σ	.025 kg s^{-2}
$C_{0,skin\text{-}oils}$	2×10^{-7} kg m^{-2}	k_{kin}	8.4×10^{25} m^3 kg^{-2} s^{-1}
m	250 amu	k_{act}	1.6×10^{16} kg^{-1} s^{-1}

ρ is the particle density ; k_{ozone} the ozone/skin-oils reaction rate constant; $k_{ozone\text{-}ex}$ the ozone/skin-oils reaction rate constant with the assumption of excess skin-oils; $C_{0,skin\text{-}oils}$ the initial concentration of skin-oils on the T-shirt; m, D, and σ the molecular mass, diffusion coefficient, and surface tension of the SVOC; $C_{SVOC,sat}$ the SVOC concentration in a saturated vapor at equilibrium; k_{kin} and k_{act} the kinetic and activation nucleation constants, respectively.

622

623 **Table 2.** Details of the experimental conditions in the chamber used for simulating particle
624 generation from ozone reactions with human clothing

Case	Ozone concentration (ppb)	Hours the T-shirt was worn (h)	Air change rate (h^{-1})
1	22	6	0.5
2	40	6	0.5
3	57	12	0.5
4	148	6	0.5
5	51	6	2.7
6	133	6	2.7

625
626

SUPPLEMENTARY MATERIALS

Model sensitivity analysis

This investigation performed a model sensitivity analysis to identify the critical modeling constants and their impact on the predictions obtained by using the thermodynamic nucleation model. We used the one-at-a-time approach while conducting the sensitivity analysis. Following this approach, we changed one constant by ±10% and kept all others at their baseline values and computed the model outputs (particle mass and number concentrations). Then we returned that constant to its baseline value and repeated the previous step for each of the other constants. Thus, we systematically studied the sensitivity of the model output to each of the model inputs.

Figures S1 is a tornado diagram representing percentage change in peak particle number concentration for Case 2 (40 ppb ozone) when the model constants were varied by ±10%. In a tornado diagram the inputs (on the y axis) are arranged systematically from top to bottom such that the ones that cause maximum variation in the output are at the top. Clearly, Figure S1 shows that the peak particle number concentration in Case 2 was the most sensitive to variations in σ, m, and ρ. Likewise, the tornado diagrams for the peak particle number concentration in Cases 1, 3, and 4 also showed similar results. Such results are due to the high sensitivity of the thermodynamic nucleation model to small changes in σ, m, and ρ since these constants appear in the exponential term of the nucleation rate expression given by Eq. (8).

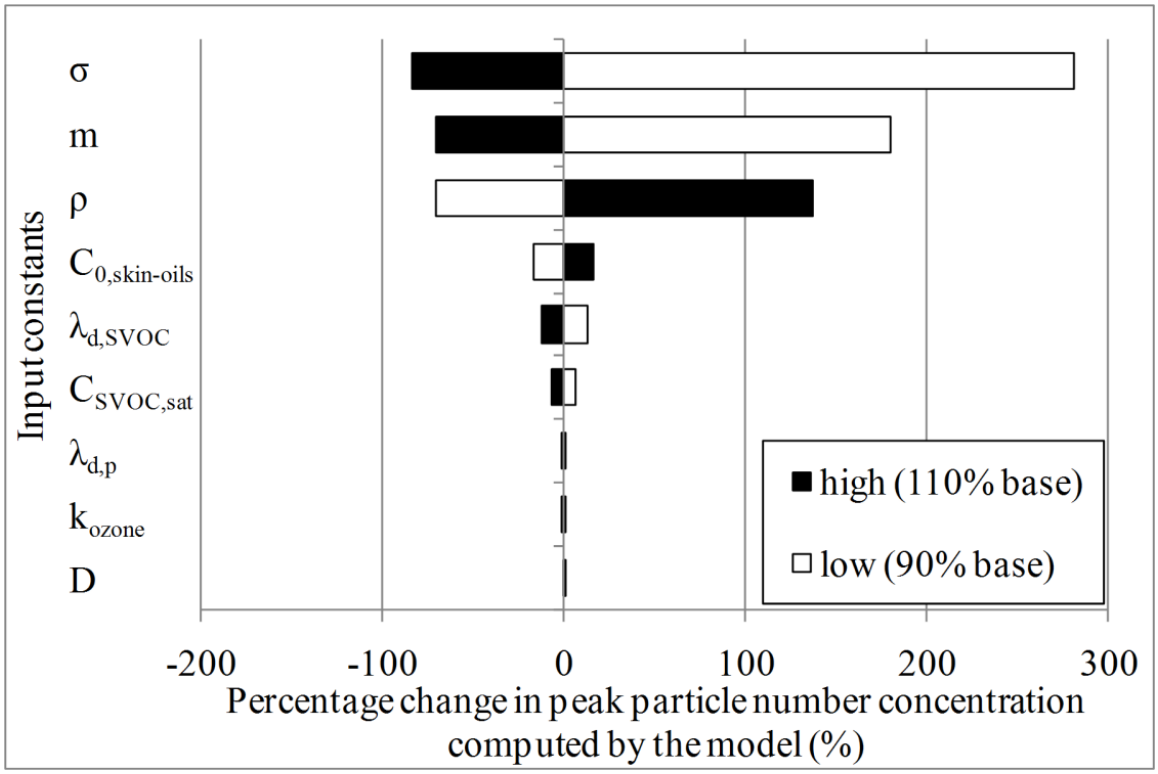

Fig. S1. Percentage change in the computed peak particle number concentration for Case 2 when the model constants were varied by ±10% from their base values given in Table 1.

Similar to the peak particle number concentration, we constructed tornado diagrams for the peak particle mass concentration in Cases 1–4. Figure S2 shows that the peak particle mass concentration was mainly sensitive to changes in σ, m, ρ, and $C_{0,skin\text{-}oils}$ in Case 2. Figure S2 also shows that the peak particle mass concentration was significantly less sensitive to the modeling constants when compared to the peak particle number concentration shown in Figure S1. This was because the particle masses were mainly controlled by condensational mass transfer from the SVOC vapor, and nucleation played a secondary role. A roughly similar trend was observed in Cases 1, 3, and 4 also.

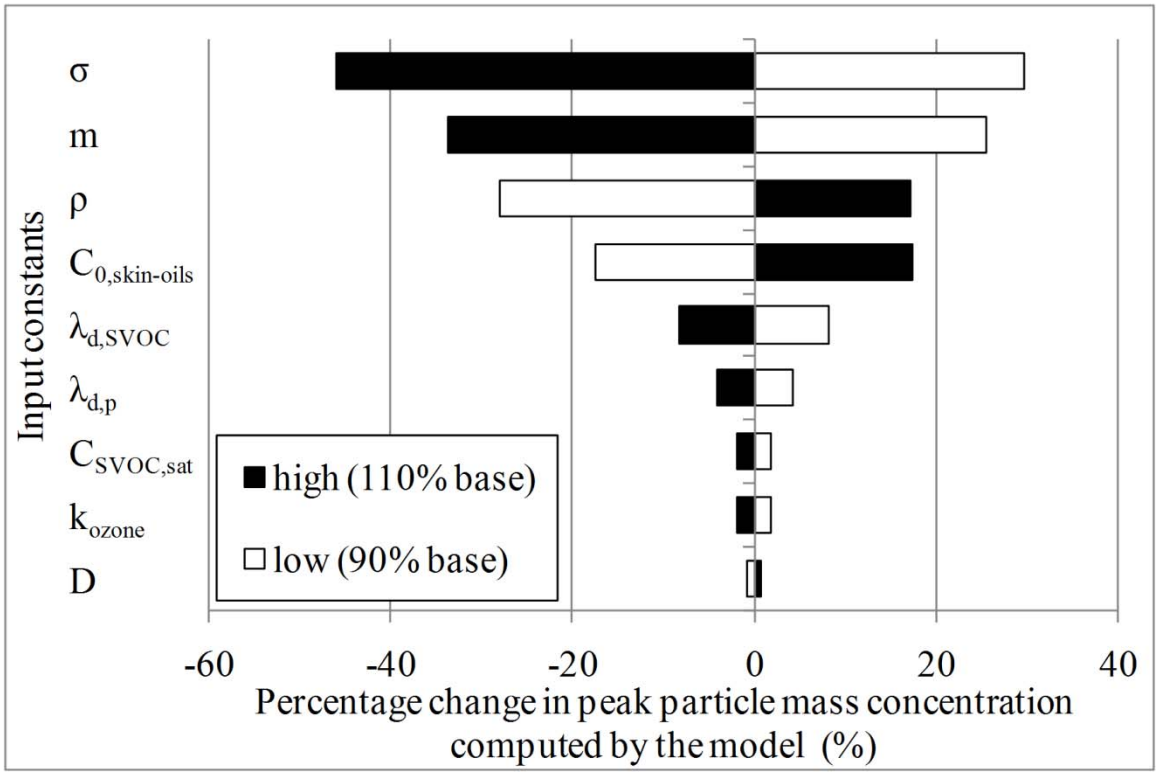

Fig. S2. Percentage change in the computed peak particle mass concentration for Case 2 when the model constants were varied by ±10% from their base values given in Table 1.